Propagation of EM Waves in Composite Bianisotropic Cylindrical Structures

Ioannis O. Vardiambasis, *Member, IEEE*, J. L. Tsalamengas, *Member, IEEE*, and Konstantinos Kostogiannis

***Abstract*—Propagation of electromagnetic waves in a bianisotropic cylinder embedded in an unbounded bianisotropic space and enclosing an array of parallel bianisotropic circular rods is studied. Based on a separation of variables technique which is facilitated by the use of suitable translation-addition relations, the analysis ends up with an infinite homogeneous system of linear algebraic equations. All matrix elements are given by pole-free, single-term, closed-form expressions. Numerical results are presented for several cases along with comparisons with previously published data. These results reveal the possibility to dynamically control the dispersion characteristics of the structure via changes in the constitutive parameters of the materials involved.**

***Index Terms*—Bianisotropic guides, composite media, cylindrical guides, optical waveguides, propagation modes.**

I. Introduction

COMPLEX media are of interest to a broad field of applications, ranging from ionospheric research and geophysical exploration, to crystal physics and integrated optics, to microwave and millimeter wave circuitry. Such media are potentially useful, in particular, in developing reciprocal and nonreciprocal microwave and millimeter-wave devices, high-efficiency microstrip antennas and arrays, guiding devices and couplers, microwave and photonic lenses, and optical filters.

In this paper, we investigate propagation in the general configuration, shown in Fig. 1, of a bianisotropic cylinder (region 1), which: 1) encloses an arbitrary number, $M_c - 1$, of parallel cylindrical bianisotropic rods [regions i ($i = 2, 3, \ldots, M_c$)] and 2) is embedded in an unbounded bianisotropic space (region 0). If desired, some regions (or all) may either be filled by isotropic or biisotropic (e.g., chiral) media or be occupied by perfect electric conductors (PECs). Although for simplicity all regions are taken to be homogeneous herein, the extension to cylindrically stratified regions is straightforward.

Some special cases shown in Fig. 2, independently treated in the past by several methods (separation of variables, coupled mode theory, and finite elements) [1]–[8], serve here to partially test the accuracy and correctness of our numerical codes.

The techniques in this paper parallel those of [9], where the corresponding nonhomogeneous (scattering) problem for an obliquely incident plane-wave excitation is addressed. The analysis in both papers ends up with infinite systems of linear, algebraic equations whose matrix elements assume closed single-term forms.

The assumed $\exp(+j\omega t)$ time dependence has been suppressed throughout the analysis.

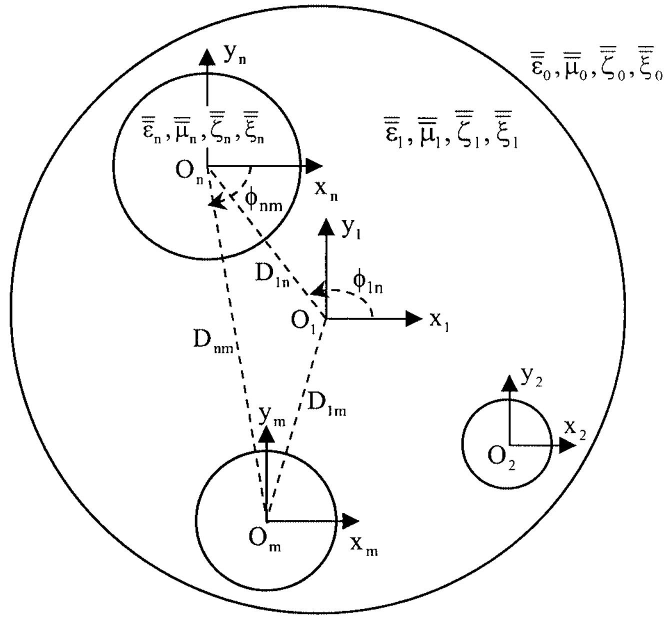

Fig. 1. Geometry of the problem: the bianisotropic cylinder $(\overline{\overline{\varepsilon}}_1, \overline{\overline{\mu}}_1, \overline{\overline{\zeta}}_1, \overline{\overline{\xi}}_1)$, embedded in the unbounded bianisotropic space $(\overline{\overline{\varepsilon}}_0, \overline{\overline{\mu}}_0, \overline{\overline{\zeta}}_0, \overline{\overline{\xi}}_0)$, encloses the bianisotropic cylinders $(\overline{\overline{\varepsilon}}_i, \overline{\overline{\mu}}_i, \overline{\overline{\zeta}}_i, \overline{\overline{\xi}}_i)$; $i = 2, 3, \ldots, M_c$.

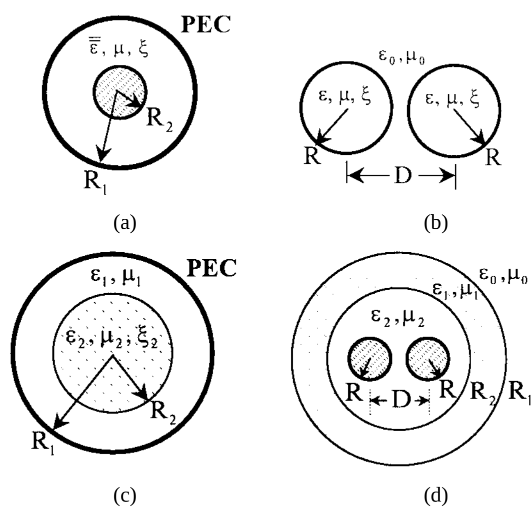

Fig. 2. (a) Coaxial gyrotropic chirowaveguide. (b) Two coupled parallel chiral rods. (c) Circular chiral/dielectric waveguide. (d) Parallel two-wire line covered with a three-layer dielectric.

Manuscript received November 30, 2001. This work was supported by the Institute of Communication and Computer Systems of the National Technical University of Athens (ICSS-NTUA) under the Archimedes 2000–01 Basic Research Project 65/37. The work of I. Vardiambasis was also supported by the State Scholarship Foundation of Greece.

The authors are with the Department of Electrical and Computer Engineering, National Technical University of Athens, GR 15773 Athens, Greece.

Digital Object Identifier 10.1109/TMTT.2003.808725

II. Basic Theory

Consider a bianisotropic medium characterized by the constitutive relations

$$\begin{aligned}\overline{D} &= \varepsilon_0 \left(\overline{\overline{\varepsilon}}\overline{E} + Z_0 \overline{\overline{\xi}}\overline{H}\right)\\ \overline{B} &= \mu_0 \left(\overline{\overline{\mu}}\overline{H} + Z_0^{-1}\overline{\overline{\zeta}}\overline{E}\right)\end{aligned} \tag{1a}$$

where $Z_0 = \sqrt{\mu_0/\varepsilon_0}$ is the intrinsic impedance of free space. Our analysis is restricted to the case where all tensors $\overline{\overline{\varepsilon}}$, $\overline{\overline{\mu}}$, $\overline{\overline{\zeta}}$, and $\overline{\overline{\xi}}$ have the form[1]

$$\overline{\overline{p}} = p_1(\hat{x}\hat{x} + \hat{y}\hat{y}) - jp_2(\hat{x}\hat{y} - \hat{y}\hat{x}) + p_3\hat{z}\hat{z}, \qquad p \equiv \varepsilon, \mu, \zeta, \xi. \tag{1b}$$

Assuming z dependence of the form $e^{-j\beta z}$, the field $\left[(\overline{E}(\overline{\rho}), \overline{H}(\overline{\rho}))\right] e^{-j\beta z}$ inside such a medium can be expressed in terms of its components along the z axis, E_z and H_z, which are found to satisfy the coupled second-order differential equations of

$$\begin{bmatrix}\nabla_t^2 E_z\\ \nabla_t^2 H_z\end{bmatrix} = \begin{bmatrix}A_1 & A_2\\ -A_2' & A_1'\end{bmatrix}\begin{bmatrix}E_z\\ H_z\end{bmatrix} \tag{2}$$

where A_1, A_2, A_1', and A_2' are constants given in [9, Appendix].

In terms of E_z and H_z, the transverse (to z) components of the field are given by

$$\begin{aligned}\begin{bmatrix}\overline{E}_t\\ \overline{H}_t\end{bmatrix} &= -\frac{1}{\Delta}\begin{bmatrix}a_1' & -a_2\\ a_2' & a_1\end{bmatrix}\\ &\quad\times\left(\begin{bmatrix}\hat{z}\times\nabla_t E_z\\ \hat{z}\times\nabla_t H_z\end{bmatrix} - \begin{bmatrix}\nu & \gamma\\ -\gamma' & \nu'\end{bmatrix}\begin{bmatrix}\nabla_t E_z\\ \nabla_t H_z\end{bmatrix}\right),\\ \Delta &= a_1 a_1' + a_2 a_2'\end{aligned} \tag{3}$$

where expressions for the constants $a_1, a_2, a_1', a_2', \nu, \gamma, \nu'$, and γ' are given in [9, Appendix].

The general solution of (2) may be written in the form

$$E_z = Z_a H_z^a + Z_b H_z^b \quad H_z = H_z^a + H_z^b \tag{4}$$

where H_z^a and H_z^b satisfy the Helmholtz equation

$$\left(\nabla_t^2 + k_q^2\right) H_z^q = 0 \; (q \equiv a, b). \tag{5}$$

[1]Gyro-electric-magnetic (gyrotropic) media, magnetized chiroferrites/chiroplasma, biisotropic (i.e., chiral), and simple (isotropic) media are, among others, some practical cases described by (1a) and (1b).

Here k_a^2 and k_b^2 denote the roots, with respect to k^2, of the biquadratic equation

$$k^4 + k^2(A_1 + A_1') + A_1 A_1' + A_2 A_2' = 0 \tag{6}$$

and

$$Z_{a,b} = \frac{(k_{a,b}^2 + A_1')}{A_2'} = -\frac{A_2}{(k_{a,b}^2 + A_1)}. \tag{7}$$

III. Representation of the Field in Region (i)

Let $[\overline{E}(\overline{\rho}), \overline{H}(\overline{\rho})]e^{-j\beta z}$ denote the field of a mode propagating in the structure of Fig. 1. We use the notation ($J_n(\cdot)$ and $H_n(\cdot)$ denote the Bessel and the second-kind Hankel functions of order n)

$$\begin{aligned}\overline{\overline{Z}}_i &\equiv \begin{bmatrix}Z_a^i & Z_b^i\\ 1 & 1\end{bmatrix}\\ \overline{\overline{J}}_n^i(\rho) &\equiv \begin{bmatrix}J_n(k_a^i\rho) & 0\\ 0 & J_n(k_b^i\rho)\end{bmatrix}\\ \overline{\overline{H}}_n^i(\rho) &\equiv \begin{bmatrix}H_n(k_a^i\rho) & 0\\ 0 & H_n(k_b^i\rho)\end{bmatrix}\end{aligned} \tag{8}$$

where the superscript i, $i = 0, 1, \ldots M_c$, is used to designate the region of space and apply separation of variables to obtain (9a)–(9c), shown at the bottom of this page. Here (a_n^i, b_n^i) and (c_n^i, d_n^i) are unknown expansion constants and (ρ_i, ϕ_i) denote the polar coordinates of $\overline{\rho}$ in the coordinate system (O_i) associated with the ith cylinder. With the help of (9a)–(9c), the other components of the field may be found via (3).

Expressions for the field, referring to the coordinate system $(O_q)(q = 1, 2, \ldots, M_c)$ exclusively, can be found from (9) using the translational-addition relations given by [9, eqs. (15)–(16)]. Then, application of the continuity conditions for the tangential components of $(\overline{E}, \overline{H})$ over all cylindrical boundaries involved yields an infinite, homogeneous, linear system of algebraic equations, which can most compactly be written in the form of (10), shown at the bottom of the following page. Here, δ_{1q} is the Kronecker delta, R_q denotes the radius of the qth cylinder, whereas the 2×2 matrices $\overline{\overline{W}}_M^1(R_q)$ and $\overline{\overline{U}}_M^1(R_q)$ coincide, respectively, with ${}^M\overline{\overline{W}}_q^J(R_q)$ and ${}^M\overline{\overline{U}}_q^J(R_q)$ of [9, eq. (20b)]. The quantities $(D_{\mathrm{sq}}, \phi_{\mathrm{sq}})$, which specify the position of O_s relative to O_q, are indicated in Fig. 1. The prime in the series over s means that the term with $s = q$ is excluded from the summation.

$$\begin{bmatrix}E_z^0(\overline{\rho})\\ H_z^0(\overline{\rho})\end{bmatrix} = \overline{\overline{Z}}_0 \sum_{n=-n_{\max}}^{n_{\max}} \overline{\overline{H}}_n^0(\rho_1)e^{jn\phi_1}\begin{bmatrix}c_n^i\\ d_n^i\end{bmatrix} \tag{9a}$$

$$\begin{bmatrix}E_z^1(\overline{\rho})\\ H_z^1(\overline{\rho})\end{bmatrix} = \overline{\overline{Z}}_1 \sum_{n=-n_{\max}}^{n_{\max}} \left[\overline{\overline{J}}_n^1(\rho_1)e^{jn\phi_1}\begin{bmatrix}a_n^1\\ b_n^1\end{bmatrix} + \sum_{s=2}^{M_c} \overline{\overline{H}}_n^1(\rho_s)e^{jn\phi_s}\begin{bmatrix}c_n^s\\ d_n^s\end{bmatrix}\right] \tag{9b}$$

$$\begin{bmatrix}E_z^i(\overline{\rho})\\ H_z^i(\overline{\rho})\end{bmatrix}_{i\neq 0,1} = \overline{\overline{Z}}_i \sum_{n=-n_{\max}}^{n_{\max}} \overline{\overline{J}}_n^i(\rho_i)e^{jn\phi_i}\begin{bmatrix}a_n^i\\ b_n^i\end{bmatrix}, \; n_{\max}\to\infty \tag{9c}$$

TABLE I

β/k_0 VERSUS TRUNCATION SIZE $n_{\max}$ FOR THE STRUCTURE OF FIG. 2(d)

$n_{\max}$	β/k_0			
	HE-1	HE-2	HE-3	HE-4
1	1.9909722	1.7775781	1.4077468	1.3328057
2	1.9909769	1.7765722	1.4077212	1.3327978
3	1.9909779	1.7765533	1.4077005	1.3327806
4	1.9909787	1.7765517	1.4076999	1.3327811
5	1.9909788	1.7765517	1.4076998	1.3327812

Vanishing the determinant of the homogeneous system (10) yields the dispersion equation of the structure. This equation is treated numerically after truncating the size of the matrix to a finite value, i.e., by considering finite values of $n_{\max}$ in (9a)–(9c). We note the following.

1) With slight modifications, the above analysis is also applicable when any region i ($i = 0, 1, 2, \ldots, M_c$) is occupied by a simple dielectric (ε_i, μ_i). In that case, in order to avoid some indeterminacies encountered in the expressions of $Z_{a,b}$, one has simply to replace $\overline{\overline{Z}}_i$ by the unit matrix $\overline{\overline{I}}$ everywhere.
2) Further simplification results when some region, say cylinder (i), is PEC. In such a case, ($\overline{E}^i, \overline{H}^i$) vanishes and thus at $\rho = R_i$ only the continuity (vanishing) of the tangential electric field needs to be accounted for.

IV. NUMERICAL RESULTS AND COMPARISONS

A. Convergence of the Algorithm Versus $n_{\max}$

The convergence characteristics of the algorithm are shown in Table I, where β/k_0 is presented versus $n_{\max}$, the truncation size of the series in (9), for the first four modes of the structure of Fig. 2(d). Region (0) is air (ε_0, μ_0), region (1) is occupied by a chiral medium ($\varepsilon_1, \mu_1, \xi_1$), region (2) is dielectric (ε_2, μ_2), and regions (3) and (4) are PECs. The parameter values are: $R_1 = 3.175$ mm, $R_2 = 0.7R_1$, $R = 0.1R_1$, $D = 0.3R_1$, $\varepsilon_1 = 2$, $\mu_1 = 1$, $\xi_1 = -\zeta_1 = j0.1$, $\varepsilon_2 = 4$, $\mu_2 = 1$, and $f = 25$ GHz. Apparently, the convergence is very rapid and stable. For instance, using $n_{\max} = 4$ suffices to obtain the propagation constant to within eight significant figures.

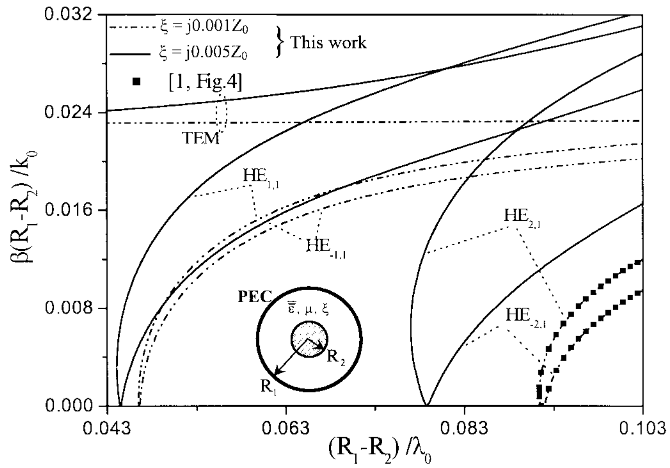

Fig. 3. $\beta(R_1 - R_2)/k_0$ versus $(R_1 - R_2)/\lambda_0$ for the first five modes of a coaxial gyrotropic chirowaveguide.

B. Dispersion Diagrams—Comparison With Previously Published Data

Fig. 3 pertains to the gyrotropic chirowaveguide of Fig. 2(a). For $\mu = 1, \overline{\overline{\varepsilon}} = (5.3361+\xi_c^2)(\hat{x}\hat{x}+\hat{y}\hat{y})-j0.1(\hat{x}\hat{y}-\hat{y}\hat{x})+(2.5+\xi_c^2)\hat{z}\hat{z}$, and for two values of the chirality parameter, $\xi = -\zeta = j0.001Z_0, j0.005Z_0$, it shows $\beta(R_1 - R_2)/k_0$ versus $(R_1 - R_2)/\lambda_0$ for several modes when $R_2 = 0.5R_1$ (λ_0 is the free-space wavelength). As seen, the effect of changing the chirality is appreciable for the dominant (TEM) as well as for the higher order modes. For the HE_{21} and HE_{-21} modes, our results are compared with those of [1] and the agreement is excellent.

Fig. 4 shows the dispersion diagrams of several modes supported by a single chiral rod of radius R (dash–dotted lines) and by two coupled parallel rods (solid lines) for the parameter values [see Fig. 2(b)] $D = 2.205R$, $\varepsilon = 1.1 + 10^{-6}Z_0^2$, $\mu = 1$, and $\xi = -\zeta = j0.001Z_0$. In the case of the single rod, our results are indistinguishable from those of [2]. Noticeably, to any mode (HE-n) of the single-rod guide correspond two HE-n modes of the double-rod guide. In other words, the HE-n modes supported by each rod when it is alone in the unbounded space couple to each other and, as a result, they appear displaced in the presence of the second rod.

Fig. 5 contains two families of plots. The first family, dotted curves, show the dispersion characteristics of the first three modes of the chiral/dielectric structure of Fig. 2(c) when $R_2 = 0.5R_1$, $\varepsilon_1 = 1$, $\mu_1 = 1$, $\varepsilon_2 = 2.81$, $\mu_2 = 1$, and $\xi_2 = -\zeta_2 = -j0.084$. These results are in full agreement with

$$\begin{bmatrix} -\overline{\overline{Z}}_q\overline{\overline{J}}_M^q(R_q) & \overline{\overline{Z}}_{1-\delta_{1q}}\overline{\overline{H}}_M^{1-\delta_{1q}}(R_q) \\ -\overline{\overline{W}}_M^1(R_q) & \overline{\overline{U}}_M^1-\delta_{1q}(R_q) \end{bmatrix}_{4\times 4} \cdot \begin{bmatrix} \begin{pmatrix} a_M^q \\ b_M^q \end{pmatrix} \\ \begin{pmatrix} c_M^q \\ d_M^q \end{pmatrix} \end{bmatrix}_{4\times 1} +(1-\delta_{1q})\sum_{n=-n_{\max}}^{n_{\max}} e^{j(n-M)\phi_{1q}} \begin{bmatrix} \overline{\overline{Z}}_1\overline{\overline{J}}_M^1(R_q) \\ \overline{\overline{W}}_M^1(R_q) \end{bmatrix} \overline{\overline{J}}_{n-M}^1(D_{1q}) \begin{pmatrix} a_n^1 \\ b_n^1 \end{pmatrix}$$

$$+\sum_{n=-n_{\max}}^{n_{\max}} {\sum_{s=2}^{L}}' e^{j(n-M)\phi_{\mathrm{sq}}} \left\{ (1-2\delta_{1q}) \begin{bmatrix} \overline{\overline{Z}}_1\overline{\overline{J}}_M^1(R_q) \\ \overline{\overline{W}}_M^1(R_q) \end{bmatrix} \overline{\overline{H}}_{n-M}^1(D_{\mathrm{sq}}) + \delta_{1q} \begin{bmatrix} \overline{\overline{Z}}_1\overline{\overline{H}}_M^1(R_q) \\ \overline{\overline{U}}_M^1(R_q) \end{bmatrix} \overline{\overline{J}}_{n-M}^1(D_{\mathrm{sq}}) \right\} \begin{pmatrix} c_n^s \\ d_n^s \end{pmatrix} = \begin{bmatrix} \overline{\overline{0}} \\ \overline{\overline{0}} \end{bmatrix},$$

$$M = 0, \pm 1, \pm 2, \ldots, \pm n_{\max}; \quad q = 1, \ldots, M_c \tag{10}$$

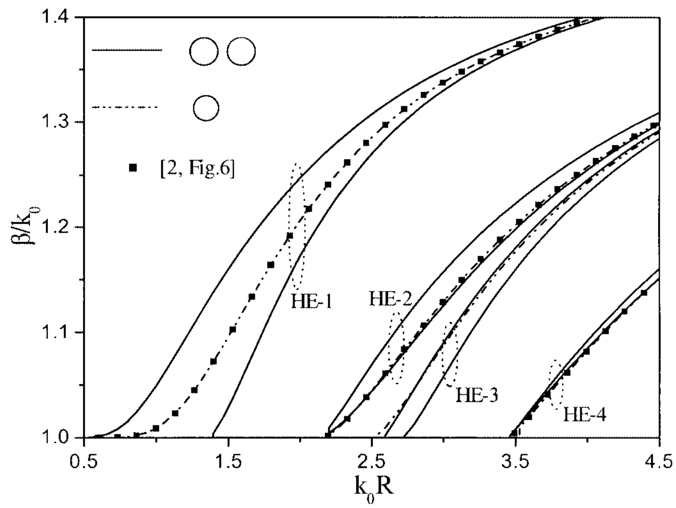

Fig. 4. β/k_0 versus k_0R. (a) Single chiral rod (dashed–dotted curves). (b) Two coupled parallel rods (solid curves).

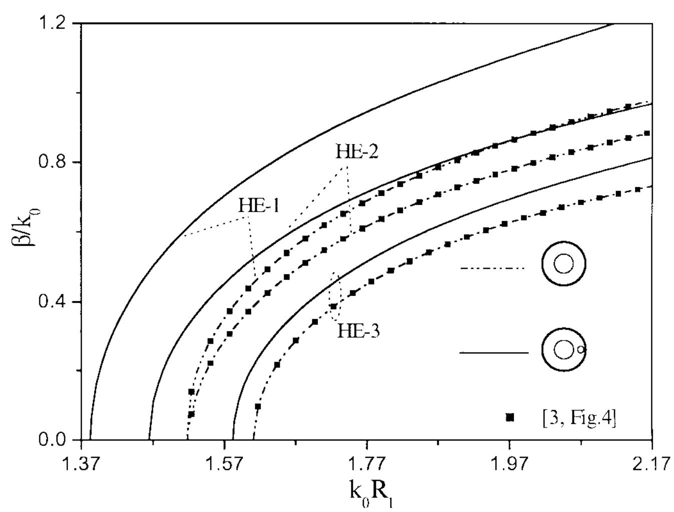

Fig. 5. β/k_0 versus k_0R_1 for the first three modes of a circular waveguide loaded by one (dotted lines) or two coupled parallel chiral rods (solid lines).

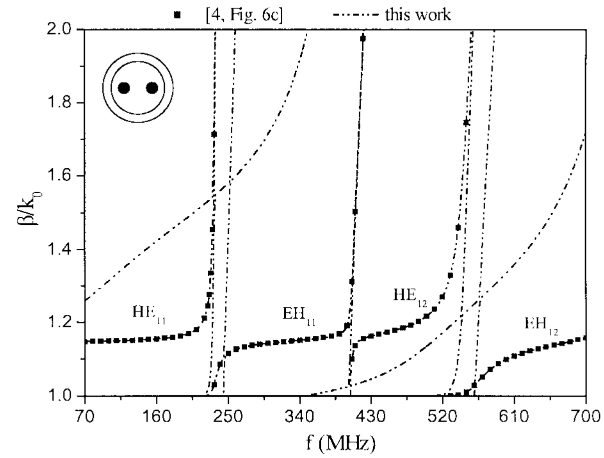

Fig. 6. β/k_0 versus frequency for several modes of the structure of Fig. 2(d).

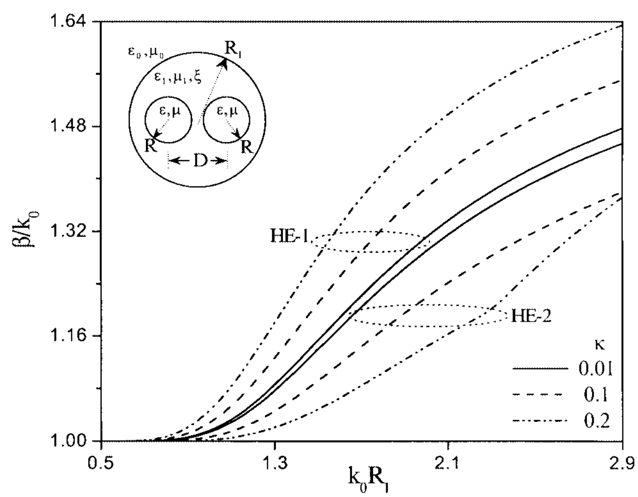

Fig. 7. β/k_0 versus k_0R_1 for the first two modes for the structure of two parallel dielectric rods coated by a chiral cylinder.

those of [3]. Note also that the first two modes, HE-1 and HE-2, have apparently the same cutoff frequency. The second family, solid curves, pertain to the case where a second chiral rod of radius $R_3 = 0.23R_1$ is placed parallel to and at a distance $0.75R_1$ from the axis of the first cylinder; its parameters are $\varepsilon_3 = 7.22$, $\mu_3 = 1$, and $\xi_3 = \zeta_3 = -j1.491$. Noticeable is the effect of this second rod on the HE-1 and HE-2 modes, which leads to considerable enhancement of the bandwidth for single-mode propagation.

Fig. 6 refers to the multiconductor-multilayered isotropic structure of Fig. 2(d). For $R_1 = 53.5$ mm, $R_2 = 6.5$ mm, $R = 0.6$ mm, $D = 7.2$ mm, $\varepsilon_1 = 79$, $\mu_1 = 1$, $\varepsilon_2 = 1$, and $\mu_2 = 1$, it shows the dispersion curves of several modes. The modes labeled HE_{11}, EH_{11}, HE_{12}, and EH_{12} have also been treated in [4]. Comparison of our results with those of [4] reveals a perfect agreement.

We note also that in validating our algorithm we were able to exactly reproduce, among others, the curves in [1, Figs. 3(a)-(c)], [2, Fig. 4], [3, Figs. 2–5], [4, Figs. 6–8], [5, Figs. 4–6], [6, Figs. 2–3], [8, Figs. 2–3] (not shown). Finally, the exhaustive comparisons which have been carried out in [9] in connection with the corresponding inhomogeneous (scattering) problem provide an alternative test of the present algorithm as well. (As noted previously, the matrix of the final algebraic system has the same form for both problems).

Fig. 7 shows β/k_0 versus k_0R_1 for the structure (see the inset) of two identical dielectric rods having $(\varepsilon, \mu) = (4.34, 1)$ and radii R, with their axes at a distance D, which are coated by an open chiral cylinder of radius R_1 when $R = 0.2R_1$ and $D = 0.5R_1$. The parameters of the chiral medium are $(\varepsilon_1, \mu_1, \xi) = (2.32, 1, j\kappa)$ where κ takes on three values, $\kappa = 0.01$, 0.1, and 0.2. Once again, we observe the radical change of the dispersion characteristics with increasing chirality.

Fig. 8 refers to the structure (see the inset) of a pair of parallel perfectly conducting cylinders coated by a magnetized ferrite cylinder. The ferrite has a relative dielectric constant $\varepsilon = 12.6$ and a tensorial relative permeability

$$\bar{\bar{\mu}} = \begin{bmatrix} \mu_1 & -j\mu_2 & 0 \\ j\mu_2 & \mu_1 & 0 \\ 0 & 0 & \mu_3 \end{bmatrix}, \qquad \mu_1 = 1 + \frac{\Omega_H}{(\Omega_H^2 - \Omega^2)};$$

$$\mu_2 = \frac{-\Omega}{(\Omega_H^2 - \Omega^2)}; \quad \mu_3 = 1. \tag{11}$$

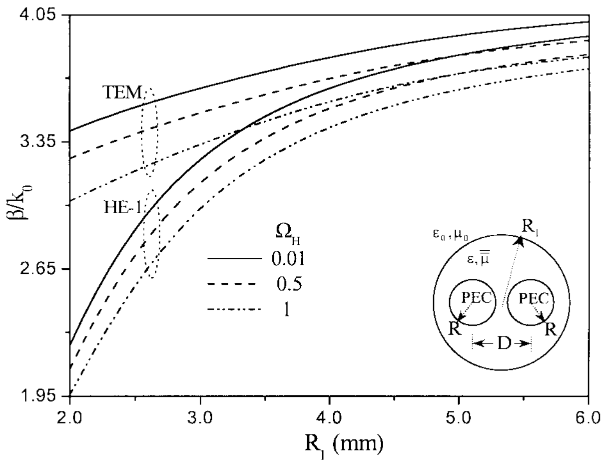

Fig. 8. β/k_0 versus R_1 for the first two modes of the structure of two parallel conducting rods coated by a ferrite cylinder. ($R = 0.6$ mm, $D = 2.8$ mm, $f = 21$ GHz).

Here $\Omega = \omega/\omega_m$, $\Omega_H = \omega_0/\omega_m$, $\omega_0 = |\gamma|\mu_0 H_0$, $\omega_m = |\gamma|\mu_0 M_0$, where H_0 is the externally applied bias (DC) magnetic field, M_0 is the intensity of the saturation magnetization, and $|\gamma| \cong 1.759 \times 10^{11}$ C/Kg. To bring to light the effect of anisotropy, we assume that $\mu_0 M_0 = 0.3$ Wb/m^2 and let Ω_H take on three values, $\Omega_H = 0.01$, 0.5, and 1. Inspection of the pertinent results reveals the possibility to dynamically control the dispersion characteristics of the structure, via a change in the externally applied dc magnetic field.

Analogous results are shown in Fig. 9 for a perfectly conducting cylinder of radius R, which is eccentrically coated by a composite cylinder of radius R_1 (chiroferrite) that obeys the constitutive relations of

$$\overline{D} = \varepsilon_0 \varepsilon \overline{E} + j\xi_c \overline{B},\ \overline{H} = j\xi_c \overline{E} + [\mu_0 \overline{\overline{\mu}}]^{-1} \overline{B}. \qquad (12)$$

Here $\varepsilon = 15$, whereas $\overline{\overline{\mu}}$ is given from (11) with $\mu_0 M_0 = 0.1$ Wb/m^2. In Fig. 9(a), we show β/k_0 versus $k_0 R_1$ for three values of Ω_H ($\Omega_H = 0.01$, 1.5, 2.5) when $\xi_c = 0.0005S$. As seen, an increase of Ω_H leads to decreasing values of β/k_0. Fig. 9(b) shows β/k_0 versus $k_0 R_1$ for three values of ξ_c ($\xi_c = 0, 0.001S, 0.002S$) when $\Omega_H = 0.3$. As seen, an increase of the chirality parameter ξ_c leads to increasing values of β/k_0.

Fig. 10 refers to a cylindrical rod, eccentrically coated by a chiroferrite cylinder [see (12)] of radius R_1 with parameters $(\varepsilon, \overline{\overline{\mu}}, \xi_c) = (12.6, \overline{\overline{\mu}}, 0.002S)$. Here $\overline{\overline{\mu}}$ has the form (11) with $\Omega_H = 1.2$ and $\mu_0 M_0 = 0.2$ Wb/m^2. The core rod of radius R is taken to be: 1) air ($\varepsilon_2 = 1, \mu_2 = 1$); 2) dielectric ($\varepsilon_2 = 12.6, \mu_2 = 1$); 3) a chiral medium ($\varepsilon_2 = 12.6, \mu_2 = 1, \xi_2 = -\zeta_2 = -j$); or 4) a PEC. In order to shed light on the nonreciprocal behavior of the structure, both β^+/k_0 and β^-/k_0 are shown versus $k_0 R_1$, β^+, and β^- being the propagation constant of the first mode propagating in the $+\hat{z}$ and $-\hat{z}$ direction, respectively. As seen, the nonreciprocal effect is very strong in all cases.

It has been proven in [10] and corroborated in [11] that a narrow, infinitely extending strip of width $2w$ is equivalent to a perfectly conducting cylindrical rod of radius $R = w/2$. Motivated by this remark, comparisons of our results have been carried out with those of [11, Fig. 4] pertaining to a pair of strips coated by a dielectric cylinder. Note that the results in [11] were based on quite different principles (singular-integral-equation methods). The agreement with [11, Fig. 4] was excellent (not shown).

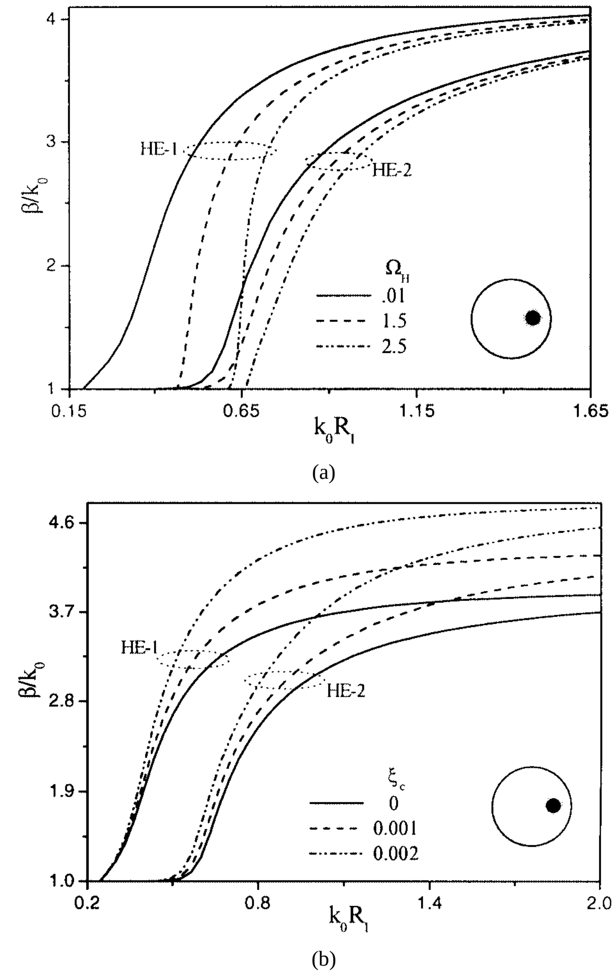

Fig. 9. β/k_0 versus $k_0 R_1$ for the first two modes of a conducting rod eccentrically coated by a chiroferrite cylinder. ($R = 0.25R_1$, $D = 0.5R_1$). (a) $\xi_c = 0.005S$ and $\Omega_H = 0.01, 1.5, 2.5$.. (b) $\Omega_H = 0.3$ and $\xi_c = 0, 0.001S, 0.002S$.

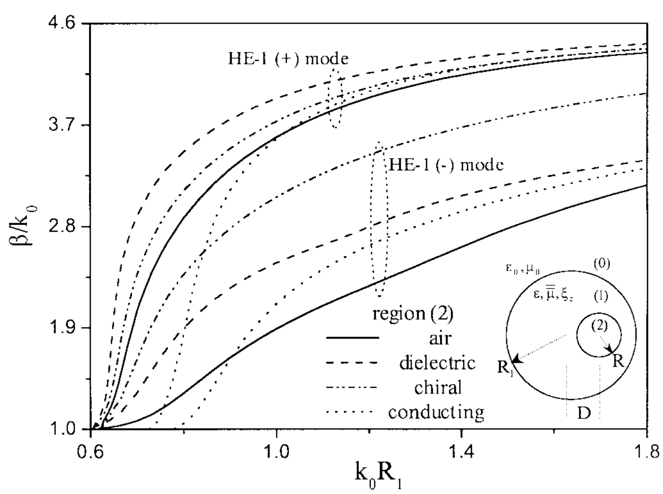

Fig. 10. β/k_0 versus $k_0 R_1$ for the first mode of a rod (dielectric, chiral or perfectly conducting) eccentrically coated by a chiroferrite cylinder. ($R = 0.5R_1, D = 0.4R_1$).

V. Conclusion

Propagation in composite cylindrical structures, composed from a bianisotropic cylinder embedded in an unbounded bianisotropic space and enclosing an array of parallel bianisotropic rods, has been investigated. To this end, a very flexible separation-of-variables technique has been used to yield linear algebraic systems whose matrix elements are given by pole-free, single-term expressions. The correctness and accuracy of the algorithm has been demonstrated by extensive comparisons with previously published data. Several numerical examples have been presented in order to demonstrate the effect of changing the constitutive parameters on the dispersion characteristics of the structure.

References

[1] Y. Wenyan, W. Wenbing, and L. Pao, "Guided electromagnetic waves in gyrotropic chirowaveguides," *IEEE Trans. Microwave Theory Tech.*, vol. 42, pp. 2156–2163, Nov. 1994.

[2] J. A. M. Svedin, "Propagation analysis of chirowaveguides using the finite-element method," *IEEE Trans. Microwave Theory Tech.*, vol. 38, pp. 1488–1496, Oct. 1990.

[3] D. Bacon and T. C. K. Rao, "Propagation modes of a cylindrical waveguide loaded by a coaxial chiral cylinder," *Proc. Inst. Elect. Eng.–Microwave Antennas and Propagat.*, vol. 145, no. 3, pp. 229–232, June 1998.

[4] Y. Kuboyama, T. Shibuya, and R. Sato, "Transmission theory of a parallel-two-wire-transmission-line covered with three layer media," *IEEE Trans. Microwave Theory Tech.*, vol. 42, pp. 264–271, Feb. 1994.

[5] P. G. Cottis, "Propagation in cylindrical guides with gyroelectric core and cladding," *Proc. Inst. Elect. Eng.*, pt. J, vol. 138, no. 6, pp. 383–388, Dec. 1991.

[6] S. F. Mahmoud, "Guided modes on open chirowaveguides," *IEEE Trans. Microwave Theory Tech.*, vol. 43, pp. 205–209, Jan. 1995.

[7] Y. Xu and R. G. Bosisio, "An efficient method for study of general bi-anisotropic waveguides," *IEEE Trans. Microwave Theory Tech.*, vol. 43, pp. 873–879, Apr. 1995.

[8] L. Valor and J. Zapata, "An efficient finite element formulation to analyze waveguides with lossy inhomogeneous bianisotropic materials," *IEEE Trans. Microwave Theory Tech.*, vol. 44, pp. 291–296, Feb. 1996.

[9] K. Konistis and J. L. Tsalamengas, "Plane wave scattering by an array of bianisotropic cylinders enclosed by another one in an unbounded bianisotropic space: Oblique incidence," *J. Elect. Waves Applicat.*, vol. 11, pp. 1073–1090, 1997.

[10] C. M. Butler, "The equivalent radius of a narrow conducting strip," *IEEE Trans. Antennas Propagat.*, vol. 30, pp. 755–758, Apr. 1982.

[11] I. O. Vardiambasis, J. L. Tsalamengas, and J. G. Fikioris, "Hybrid wave propagation in generalized Goubau-type striplines," *Proc. Inst. Elect. Eng.–Microwave Antennas and Propagat.*, vol. 144, no. 3, pp. 167–171, June 1997.

Ioannis O. Vardiambasis (M'01), photograph and biography not available at the time of publication.

J. L. Tsalamengas (M'87), photograph and biography not available at the time of publication.

Konstantinos Kostogiannis, photograph and biography not available at the time of publication.